minerals

MDPI

Article

Primary and Secondary Geochemical Signals in the Chemical Composition of Exoskeleton of *Corumbella werneri* (Tamengo Formation, Corumbá Group, Brazil): A Pilot Study

Ana Valéria Alves Calmon Almeida *, Martino Giorgioni *, Detlef Hans Gert Walde, Dermeval Aparecido Do Carmo and Guilherme de Oliveira Gonçalves

Universidade de Brasília, Instituto de Geociências, Programa de Pós-graduação em Geologia, Brasilia 70910-900, Brazil; derme@unb.br (D.A.D.C.)

* Correspondence: calmonvals@gmail.com (A.V.A.C.A.); gmartino@unb.br (M.G.)

Abstract: The study of Neoproterozoic carbonate sequences is complicated due to several variables influencing the geochemical and mineralogical composition, compounded by the scarcity of environmental analogs. The Tamengo Formation in the Corumbá Group is one of the most extensively studied archives of the Neoproterozoic in South America and encompasses Ediacaran guide fossils of *Corumbella werneri* and *Cloudina lucianoi*. This research focused on a marl sample containing well-preserved bioclasts of exoskeletons of *Corumbella werneri*, which is one of the earliest biomineralizing organisms. By utilizing diverse techniques such as optical and SEM microscopy, QEMSCAN imaging, electron microprobe, in situ ICP-MS, and isotope analyses, this study reveals primary and secondary signals in the bioclastic exoskeletons and the matrix within. These findings shed light on the sedimentary environment and diagenetic history of the Tamengo Formation. It is revealed that *Corumbella werneri* likely inhabited calm conditions, just below the base of storm waves and above a sharp chemocline at the bottom. In addition, the presence of distinct hydrothermal signals in the composition of REEs indicates a potential magmatic event that occurred in the region after the deposition of the succession. This pilot study highlights that the history recorded in the Neoproterozoic rocks of the Tamengo Formation is complex, and thus more detailed studies integrating lithological, paleontological, and geochemical parameters are necessary to reach a correct interpretation of this sequence.

Keywords: Marlstones; Ediacaran; *Corumbella werneri*; Paraguay Belt; Corumba Group; Isotopes; REE

check for updates

Citation: Calmon Almeida, A.V.A.; Giorgioni, M.; Walde, D.H.G.; Do Carmo, D.A.; Gonçalves, G.d.O. Primary and Secondary Geochemical Signals in the Chemical Composition of Exoskeleton of *Corumbella werneri* (Tamengo Formation, Corumbá Group, Brazil): A Pilot Study. *Minerals* **2024**, *14*, 784. https://doi.org/10.3390/min14080784

Academic Editors: Olev Vinn and Dominic Papineau

Received: 18 March 2024
Revised: 18 June 2024
Accepted: 24 June 2024
Published: 31 July 2024

Copyright: © 2024 by the authors. Licensee MDPI, Basel, Switzerland. This article is an open access article distributed under the terms and conditions of the Creative Commons Attribution (CC BY) license (https://creativecommons.org/licenses/by/4.0/).

1. Introduction

The Neoproterozoic spans the geological time interval between 1 Ga and 0.538 Ga [1]. During this era, tectonic, climatic, and environmental events have imparted their signatures in the chemical and sedimentary archives of carbonate rocks [2–7].

Investigations utilizing elemental and isotopic geochemistry play a pivotal role in deciphering Precambrian sequences; however, they are made particularly complex by the paucity of analogs with present-day settings, both in terms of biota and environmental conditions [8]. Additionally, the original chemical and isotopic composition of the rocks may undergo modifications during diagenesis, due to interactions between rocks and fluids as well as changes in temperature and pressure [9,10]. Therefore, a proper interpretation of geochemical signals in Neoproterozoic records requires a thorough characterization of the lithofacies and mineralogical and geochemical properties of a rock. Consequently, it requires an approach that integrates sedimentologic, petrographic, mineralogical, and geochemical parameters to constrain the different variables.

The Corumbá Group, situated in the western region of Brazil within the geological context of the Paraguay Belt, underwent a complex geological history, transitioning from a rift-type basin to a passive margin [11–13]. The rocks of the Tamengo Formation, occurring in the upper part of this group, are one of the most studied records of the Neoproterozoic

in South America, and are particularly known for yielding some of the earliest organisms with mineralized exoskeletons, including *Corumbella werneri* Hahn et al.,1982 [14] *Cloudina lucianoi* [15], and *Cloudina carinata* Cortijo et al., 2010 [16,17].

In this research, a sample of the Tamengo Formation containing exceptionally well-preserved bioclasts of *Corumbella werneri* was studied. It integrated different petrographic, geochemical, isotopic, and mineralogical parameters measured from the exoskeletons of *Corumbella werneri* and the matrix in-between to identify the primary and secondary signals. Notably, this investigation addresses a research gap, providing substantial insights into the mineralogical, elemental, geochemical, and isotopic characteristics of *Corumbella werneri* exoskeletons and the associated rock. It is revealed that both primary and secondary signatures are recorded in the studied sample, indicating that *Corumbella werneri* probably lived in a calm environment, just below the storm wave base and above a sharp and shallow chemocline. In addition, a magmatic event might have occurred at a regional scale during or after the burial of the Tamengo Formation.

2. Geological Settings

The southern portion of the Paraguay Fold Belt comprises units from the Cuiabá Group and Puga Formation. In addition, there are rocks from the Jacadigo Group and the carbonate and siliciclastic rocks of the Corumbá Group (Figure 1A; [11–13]). The sedimentation of the Corumbá Group took place after the breakup of the Rodinia Supercontinent at the end of the Neoproterozoic. It is characterized, from bottom to top, by the Cadieus, Cerradinho, Bocaina, Tamengo, and Guaicurus formations [18–20].

Among the association of carbonate and siliciclastic rocks of the Corumbá Group, the Tamengo Formation stands out, especially for its fossil content. The presence of two guide fossils, *Cloudina lucianoi* and *Corumbella werneri,* allows for the positioning of the Tamengo Formation in the uppermost Ediacaran [13,17,18,21,22]. This age is corroborated by the absolute dating of [23,24], with a U-Pb age on volcanic ash of around 542 $\pm$ 0.32 Ma (2 s).

The Tamengo Formation represents a neritic marine environment from shallow to deep settings [12,13,21,22]. Its basal portion comprehends breccias and sandstones, transitioning to dolostones and limestones, and concluding with marls and shales [13,25,26]. This unit exhibits two facies associations: (i) shoreface with oolitic bars and (ii) offshore influenced by storms [27,28].

In the Porto Sobramil section, Figure 1B, the highlighted layers represent the upper portion of the Tamengo Formation. In this context, three distinct levels of siltstones and mudstones are identified, showcasing the presence of *Corumbella werneri.* These strata alternate with limestones where the occurrence of *Cloudina lucianoi* is documented (Figure 1C; [17]).

The authors of [14] proposed a new Subclass, Corumbellata, within the Order Corumbellida and the Family Corumbellidae due to the morphological complexity of the organism. Some researchers classified *Corumbella werneri* as a vendobiont, a group with a brief existence in the late Neoproterozoic, while others compared its features to conulariids or coronates in the Class Scyphozoa, Phylum Cnidaria [29–31]. However, recent studies such as [32] discuss and question the previous classification based on taphonomic and morphological considerations.

Although there have been many related studies, the classification, preservation, and other aspects related to the life behavior of *Corumbella werneri* also remain shrouded in mystery. In [27] the authors use the fossils found in the Tamengo Formation as a foundation to investigate aspects related to sedimentation and position on the carbonate ramp, proposing that the muddy rocks and impure limestones containing exoskeletons of *Corumbella werneri* originated from an outer ramp.

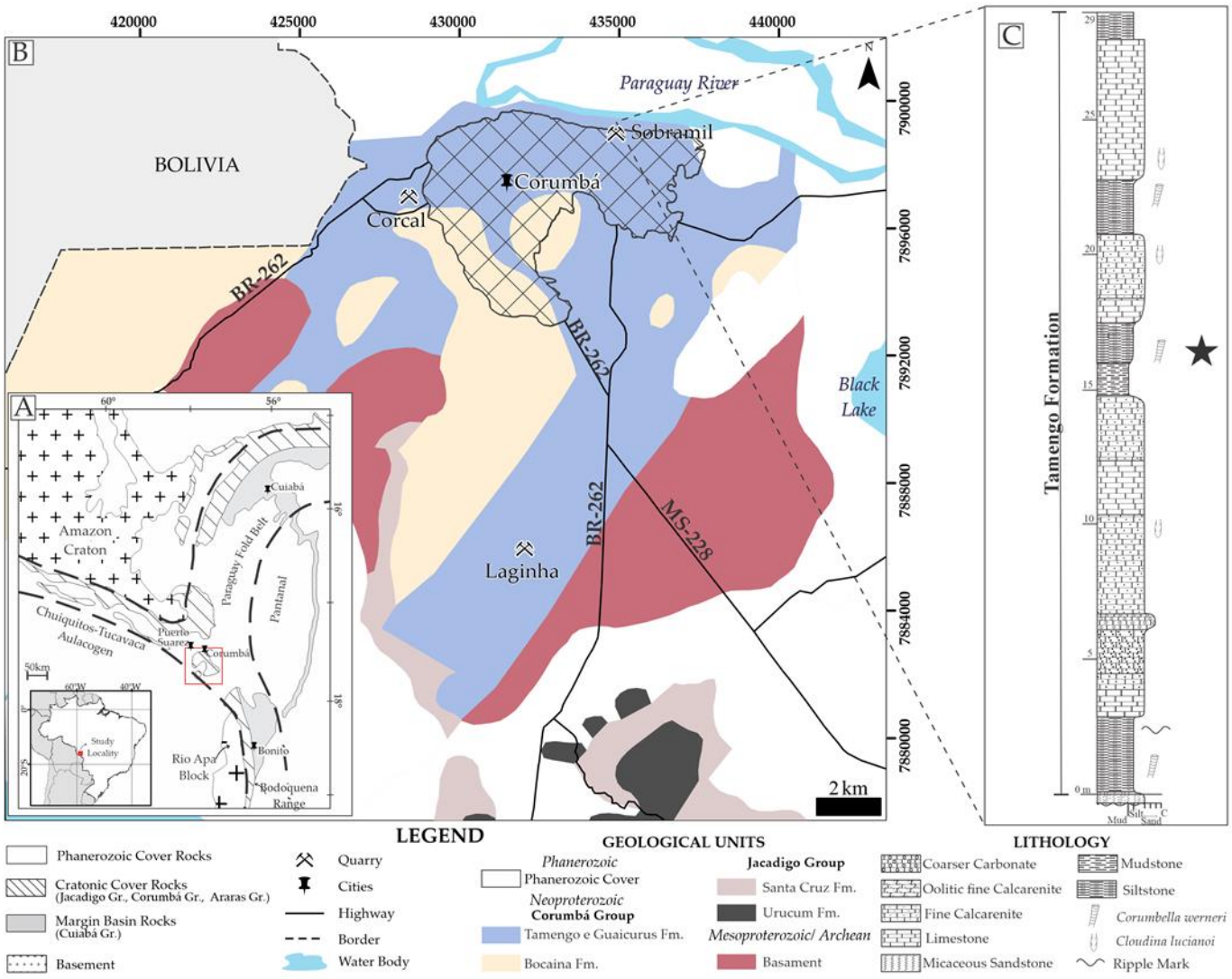


Figure 1. (**A**) Geological Map of the Paraguay Belt with emphasis on the studied area (red rectangle), modified from [33]; (**B**) Geological Map and Location of the study section, modified from [33]; (**C**) Section of the Sobramil Quarry with emphasis on the sample location (black star), adapted from [17].

3. Materials and Methods

This study uses geochemical and mineralogical analyses on a sample containing well-preserved fragments of the exoskeleton of *Corumbella werneri* to identify the signal of paleoenvironmental and post-depositional processes. The material was selected considering the occurrence of *Corumbella werneri* fragments with particularly good preservation to identify the most pristine signals. Most of the time, the specimens of *Corumbella werneri* in the Tamengo Formation occur as molds or in an oxidized form without retaining the original exoskeleton; therefore, the sample selected for this study is of a rare kind, with exceptionally good preservation. This sample is housed at the Museum of Geosciences at Research Collection, under the acronym CP.

The sample was sectioned into five slices, one of which was used for a polished thin section while the other four were mounted in resin and then polished. Three sections were created, two with a single sample piece each and one with two discrete pieces.

3.1. Petrographic Analysis

Macroscopic evaluation included an assessment of textural aspects and potential evidence of sedimentary and diagenetic structures. Microscopic observations were conducted in the Micropaleontology Laboratory at the University of Brasilia using a Zeiss Axioscope 5 optical petrographic microscope equipped with ZEISS (Oberkochen, Germany) Zen 3.4 software to identify compositional, textural, and diagenetic features [34].

3.2. Mineralogical Analyses

The investigation was conducted at the Quantitative Electron Microprobe Laboratory (QEMLab) at the University of Brasilia. The instrumental platform employed was the QUANTA FEI 650F, model QEMSCAN, equipped with two Energy-Dispersive X-ray Spectroscopy (EDS) detectors of the BRUKER XFLASH model. Analysis conditions for the generation of geochemical maps were set at a voltage of 15 kV, a current of 10 nA, and under high vacuum.

For the analysis of field images, the specified parameters encompassed a pixel spacing of 10 μm, a count of 3000 per pixel, and an average analysis duration of seven hours. After the analytical phase, the sample underwent processing through IDiscover 5.3, utilizing the QEMLab's internal Species. A bespoke identification protocol was formulated in this research, necessitating modifications to the laboratory's internal SIP (Oil & Gas SIP List). The minerals were systematically categorized into four primary groups: calcite, quartz, clay minerals, and accessory minerals. A necessity for reclassification arose due to the clay minerals' granulometry being smaller than the machine's beam size (>10 μm) [35].

3.3. Electron Microprobe

The analyses were conducted to chemically characterize major and minor elements present in both the exoskeletons and matrix of the rock. This investigation aimed to determine the concentrations of twelve elements, Mg, Al, Si, K, Ca, P, Ti, Mn, Fe, Ba, Sr, and V, in the exoskeleton and the matrix, separately. The study employed a JEOL-JXA-8230 microprobe (Tokyo, Japan) located in the Electron Microprobe Laboratory at the University of Brasilia. The analytical conditions included an electron beam acceleration of 15 kV with an electric current of 5 nA.

3.4. Trace and Rare Earth Elements

Trace element compositions were obtained at the Laboratory of Geodynamics, Geochronology, and Environmental Studies (LEGGA) of the University of Brasilia using a Thermo Finningan Element XR high-resolution single-collector sector field ICP-MS coupled to a 193 nm Iridia laser ablation system. Analyses were performed on both exoskeletons and the matrix, separately. The spots were taken cautiously in order to avoid overlap between the two constituents, which are both larger than the beam size. The following masses were analyzed: ^{25}Mg, ^{29}Si, ^{43}Ca, ^{47}Ti, ^{55}Mn, ^{59}Co, ^{60}Ni, ^{63}Cu, ^{66}Zn, ^{85}Rb, ^{88}Sr, ^{89}Y, ^{95}Mo, ^{137}Ba, ^{139}La, ^{140}Ce, ^{141}Pr, ^{143}Nd, ^{147}Sm, ^{151}Eu, ^{157}Gd, ^{159}Tb, ^{163}Dy, ^{165}Ho, ^{166}Er, ^{169}Tm, ^{172}Yb, ^{175}Lu, ^{177}Hf, ^{208}Pb, ^{232}Th, and ^{238}U. Each mass was measured for 10 ms during 49 runs. The laser parameters included an ablation spot size of 50 μm for the samples and 20 μm for the reference materials, a laser fluence of 2.0 J/cm², and a laser repetition rate of 20 Hz. Each spot analysis consisted of 20 s of sample ablation and 10 s of background measurement.

The primary reference material was SRM NIST612 glass [36] and the reference materials used for quality control were SRM NIST610 glass [36], Diamantina monazite [37], and Durango apatite [38]. The results were processed through Iolite 4.0 [39] as time-resolved signals. The internal reference value used for calibration was stoichiometric CaO (40 wt. %) for the carbonate samples, CaO (20 wt. %) for the Durango apatite, and Ce_2O_3 (28 wt. %) for the Diamantina monazite. The precision of multiple analyses of the quality control reference material is better than 5% for most elements and agrees within uncertainty with published data from [36–38].

3.5. C and O Isotopes

C and O isotope compositions were obtained at the Laboratory of Geodynamics, Geochronology, and Environmental Studies (LEGGA) of the University of Brasilia. The exoskeleton of *Corumbella werneri* and the matrix were sampled separately utilizing micro-scale perforations on the polished surfaces. The matrix was sampled at 7 points and the exoskeletons at 5 points. After microdrilling, 0.2 mg aliquots from each sample were precisely weighed and enclosed in sealed glass tubes equipped with caps and septa. These tubes were subsequently introduced into the Gas Bench II apparatus, undergoing a flushing process to remove atmospheric air and replace it with helium.

Following the flush, the samples underwent a reaction with 99% H_3PO_4 at a controlled temperature of 72 °C. The resultant CO_2 gas from the reaction was then directed through the gas flow controller Conflo IV and subsequently to the IRMS Delta V Plus, enabling the precise determination of the isotopic ratios of C and O in the gas. The reported results are expressed in delta notation relative to the Vienna Pee Dee Belemnite (VPDB) standard [40], meticulously calibrated against the international standard NBS-19 and an in-house CABRA (Carrara marble from Brasília) reference material.

3.6. Sr Isotopes

The determination of strontium isotopic ratios was conducted at the Laboratory of Geodynamics, Geochronology, and Environmental Studies (LEGGA) of the University of Brasilia. For the analysis of strontium isotopes ($^{87}Sr/^{86}Sr$), samples were collected from selected surfaces with laser ablation (LA), utilizing an Analyte Excite ArF 193nm coupled to a multi-collector (MC)-ICP-MS Neptune XT. The exoskeleton of *Corumbella werneri* was sampled from 45 points on a mount (Figure S1), whereas the matrix was sampled from 25 points on a thin section (Figure S2). The matrix sampled from the mount did not yield reliable values.

The analyses were performed with a spot diameter of 110 μm, operating at a frequency of 20 Hz, and employing a nominal energy of 4.72 J/cm^2. The ablated aerosol was purged from the HelEx II laser cell using 0.71 L/min (0.35 + 0.35) of helium. The Neptune XT was employed, equipped with nine Faraday detectors measuring masses from 82 to 88 in static mode with amplifiers of 10^{11} Ω. The Neptune XT is equipped with the Jet interface, a combination of a high-efficiency dry mechanical pump and a mix of "Jet" and "X" cones, enhancing sensitivity during the analytical session as reported by [41,42].

Background measurements were taken 10 s before each ablation, followed by data acquisition for 30 s. Raw data were integrated every 1.031 s. Mass bias was corrected by normalizing to $^{86}Sr/^{88}Sr$ = 0.1194. Rb and Kr interferences were corrected using the exponential law and the natural $^{87}Rb/^{85}Rb$ = 0.38560, $^{84}Kr/^{83}Kr$ = 4.95565, and $^{84}Kr/^{83}Kr$ = 1.5026 ratios. Any residual bias was corrected by normalizing to an in-house otolith (OTH; ID-TIMS $^{87}Sr/^{86}Sr$ = 0.70912) reference material, representative of the isotopic composition of modern oceanic water (0.70918, for example [43,44]). Walnut Canyon calcite [45] was used for quality control. Raw data were processed using Iolite 4.0 [39] and the Sr Universal DRS [46].

4. Results

The results presented below include characterization of the petrography, chemical composition, rare earth elements (REE), and Sr, C, and O isotopes of the exoskeletons of *Corumbella werneri*. Supplementary Materials providing further details is available.

4.1. Petrography

The studied sample has a clastic texture with a clear, yellowish-to-brown/gray matrix and bioclasts with a dark gray color (Figure 2A). Approximately 10 to 15% of the bioclasts are elongated, semi-cylindrical forms, originating from fragments of the fossilized exoskeletons of *Corumbella werneri.* Fragments range from 1 mm to 5 mm, with a predomi-

nance of 3 mm; however, there are also occasional fragments of 7 mm dispersed randomly (Figure 2B).

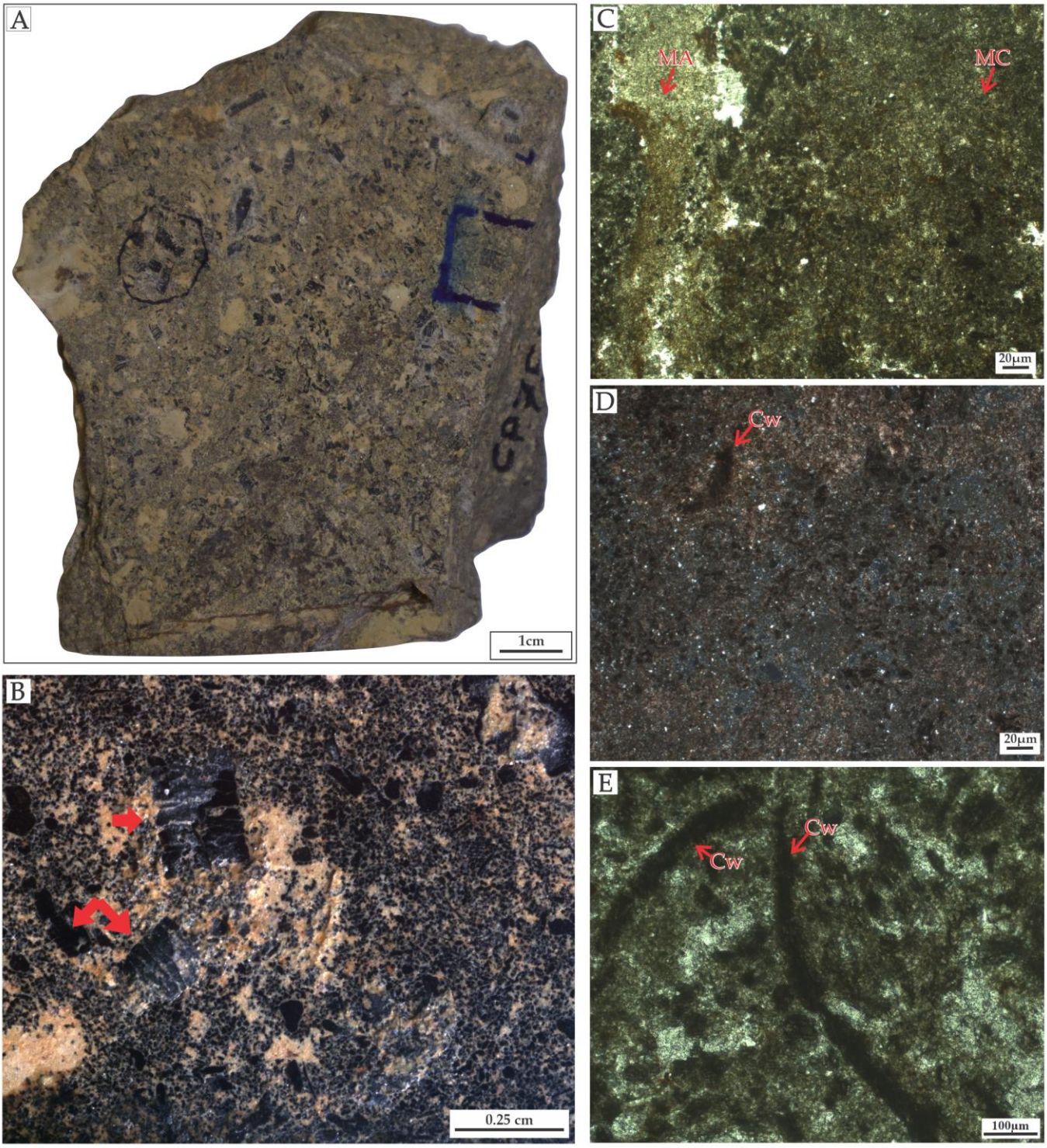


Figure 2. (**A**) Hand sample showing well-preserved exoskeletons of *Corumbella werneri* in the marked areas; (**B**) Close-up photo of the hand sample revealing two well-preserved fragments of *Corumbella werneri* on the left side of the image; (**C**–**E**) are photomicrographs where: (**C**) Illustrates the interaction between carbonate and clayey matrices; (**D**) Displays the mixture of the carbonate matrix (MC, darker brown) with the clayey matrix (MA, lighter gray), and the exoskeleton of *Corumbella werneri* (Cw) in crossed nicols; (**E**) Detailed view of the exoskeletons of *Corumbella werneri*.

Microscopically, the rock consists of 80% matrix, 15% fragments of *Corumbella werneri*, and 5% extraclasts. The matrix has a marly composition, consisting of 50% brownish micrite and 30% grayish clay. Both constituents are homogeneously distributed throughout the rock (Figure 2C,D).

Bioclastic fragments vary in size from ~0.25 cm to ~0.4 cm and are predominantly larger than 0.3 cm. They usually present a cylindrical shape and a thin wall (Figure 2E). Additionally, extraclasts of quartz, with an average size smaller than 0.5 mm and an irregular shape, are observed. The rock does not show significant sedimentary structures.

Microscopic analysis did not reveal significant secondary features in the texture and composition of the rock matrix. As for the bioclasts, they show evidence of fragmentation due to clastic transport, but no diagenetic alteration. SEM analyses also revealed no post-depositional textures, such as sparry calcite and well-developed cements. Only occasional minor compositional modifications were observed in the exoskeletons, evidenced by micrometric crystals of authigenic pyrite (Figure 3A) and silicification (Figure 3B).

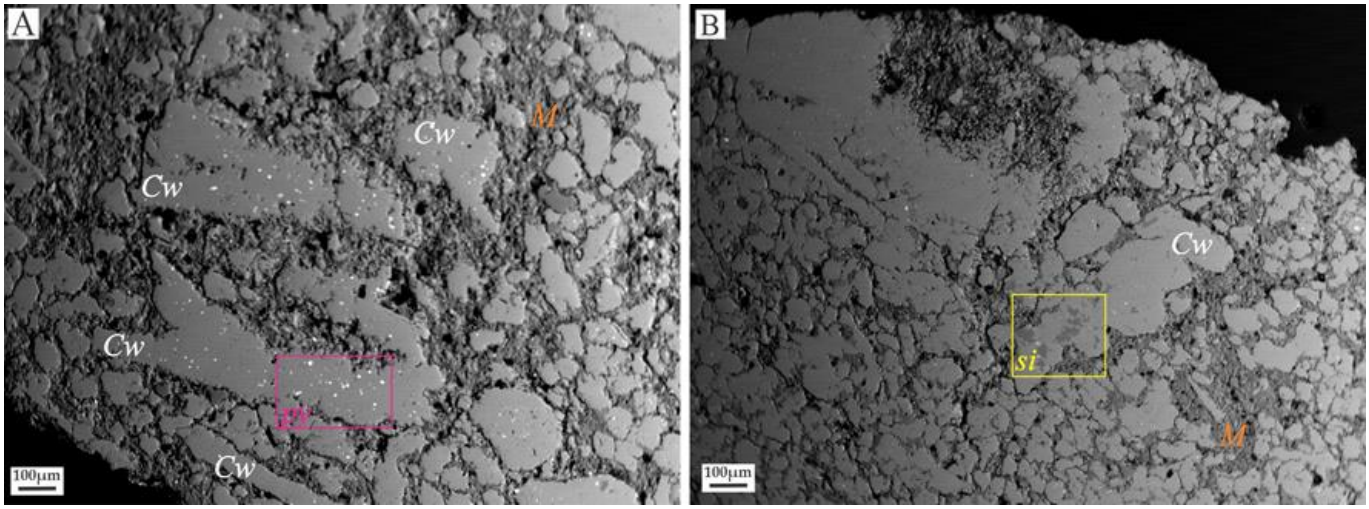


Figure 3. Microprobe Image of the Marl, where Cw—*Corumbella werneri* and M—matrix. (**A**) Pyritization of the exoskeleton with micrometric pyrite crystals (py); (**B**) Silicification of the exoskeleton (si).

Mineral imaging using QEMSCAN was applied to better visualize mineral phases (Figure 4) and understand the arrangement and interaction of constituents. The mineralogical composition consists of approximately 58% calcite, 19% quartz, 17% clay minerals, and 5% pores. Additionally, accessory minerals (<0.2%) such as rutile, K-feldspar, zoisite, dolomite, pyrite, and apatite are observed in the rock. Based on the textural and compositional observations, the rock can be classified as a bioclastic packstone with a marly matrix [47,48].

4.2. Chemical Composition

The graphs in Figure 5 were generated from the data obtained with electron microprobe analysis to compare the abundance of major and minor elements between the matrix and the exoskeleton fragments of *Corumbella werneri.* The exoskeleton fragments are predominantly calcitic, with values of CaO mostly higher than 95%. Although it is sometimes slightly lower, it still remains above 85%. When CaO values are below 95%, there is an increase in terrigenous elements such as aluminum and silica, which are more abundant in the matrix. Therefore, in the few spots with lower values of CaO, there might have been a little contamination from the matrix lying below the bioclast during the analysis. This contamination, however, does not change the main composition of the constituents. The other elements show much lower percentages and are classified as minor and trace elements depending on their concentrations.

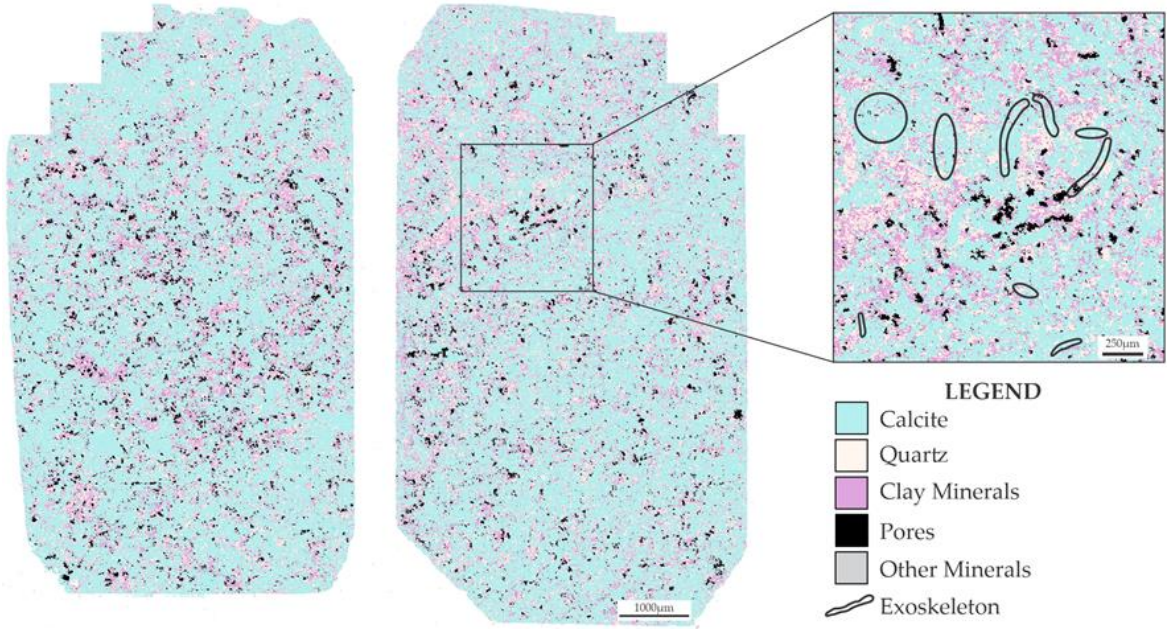


Figure 4. QEMSCAN image. It is possible to observe, in the close-up image, the mineralogical interaction with the exoskeletons of *Corumbella werneri*.

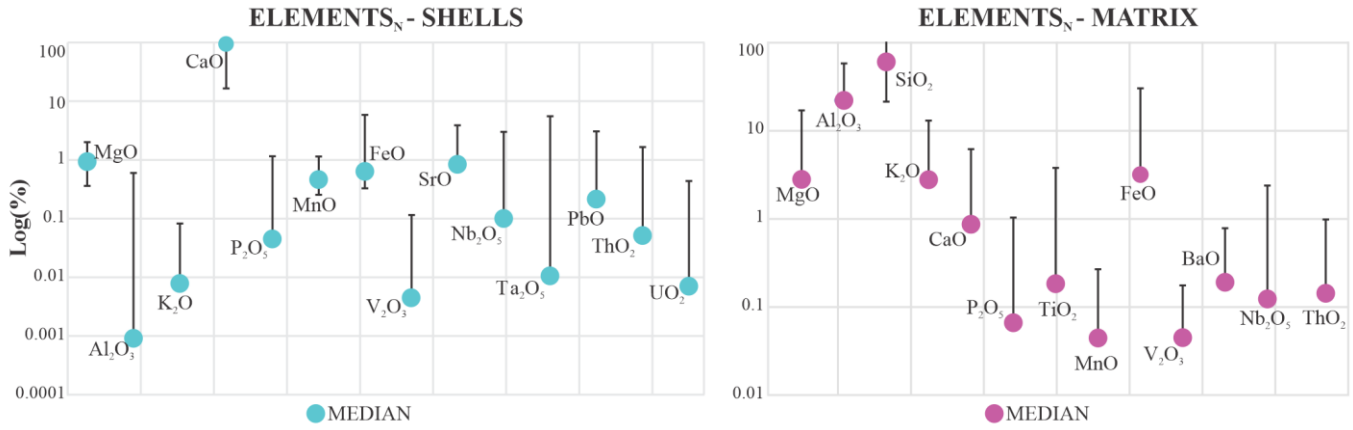


Figure 5. Distribution of the maximum, minimum, and median content of the analyzed elements in the constituents.

More significant elemental variability was identified in the matrix, with oscillating values, especially of SiO_2 and Al_2O_3. These elements can be the signal of terrigenous minerals such as quartz and clay minerals, as evidenced in the petrographic and QEMSCAN data. MgO, CaO, FeO, MnO, BaO, K_2O, and TiO_2 were observed in smaller amounts.

The matrix showed a significant siliciclastic contribution. The Pearson coefficients in the rock matrix (Table 1) were fairly good ($P > 0.4$) between Al_2O_3 vs. MgO, Al_2O_3 vs. K_2O, and MgO vs. FeO, which can be explained by the compositional variations in clay minerals. Meanwhile, the correlations of CaO vs. MgO and CaO vs. FeO are considered moderate ($P \geq 0.4$) and can be explained by the influence of the micritic fraction, which occurs in smaller quantities in the matrix and may undergo diagenetic alterations.

Table 1. Positive (blue) and negative (red) correlations for major and minor elements of the Matrix.

	MgO	Al_2O_3	SiO_2	K_2O	CaO	TiO_2	MnO	FeO	BaO
MgO	1	0.49	−0.49	0.03	−0.12	−0.07	0.21	0.67	−0.06
Al_2O_3	0.47	1	−0.90	0.53	0.10	0.16	−0.02	0.30	0.23
SiO_2	−0.49	−0.90	1	−0.54	−0.25	−0.14	−0.16	−0.63	−0.25
K_2O	0.00	0.53	−0.54	1	−0.28	0.32	0.14	−0.01	−0.01
CaO	0.40	0.10	−0.25	−0.28	1	−0.28	−0.13	0.41	0.05
TiO_2	−0.09	0.16	−0.14	0.32	−0.28	1	0.16	−0.16	−0.17
MnO	0.31	−0.02	−0.16	0.14	−0.13	0.16	1	0.24	−0.14
FeO	0.66	0.30	−0.63	−0.01	0.41	−0.16	0.24	1	0.34
BaO	−0.02	0.23	−0.25	−0.01	0.05	−0.17	−0.14	0.34	1

A strong negative correlation (P > 0.9) between SiO_2 and Al_2O_3 was observed, indicating that these two elements can be associated with two different terrigenous phases, such as SiO_2 to quartz and Al_2O_3 to clay minerals. Similarly, minor anticorrelations between SiO_2 vs. MgO, SiO_2 vs. K_2O, and SiO_2 vs. FeO may occur due to chemical variations within the clay minerals.

The exoskeleton exhibits very high values of CaO, with it being the only major element. The established correlations between the minor elements MnO vs. FeO and MgO vs. FeO showed low correlation levels (P = −0.3), suggesting a low diagenetic alteration of the chemical composition (Table 2).

Table 2. Positive (blue) and negative (red) correlations for major and minor elements in the exoskeletons of *Corumbella werneri*.

	MgO	CaO	MnO	FeO
MgO	1	0.2	0.7	−0.3
CaO	0.2	1	0.01	−0.4
MnO	0.7	0.01	1	−0.3
FeO	−0.3	−0.4	−0.3	1

The correlation between CaO vs. FeO is also negative and very small (P = −0.4), but this relationship may be attributed to the presence of pyrite in the fossils. Finally, the correlation between MnO vs. MgO can be explained by the very limited presence of dolomite, which may represent diagenetic alterations.

4.3. Rare Earth Elements (REEs)

The analyses of trace elements, rare earth elements, and some indices of the fossil and the matrix are presented in Table 3. The Europium anomaly (Eu/Eu*) was calculated using the expression ($2 \times Eu_N/Sm_N + Gd_N$) in [49], where N signifies values normalized to PAAS [50]. For a better visualization of the data patterns, separate graphs were generated for the two analyzed constituents.

In general, the analyzed sample shows a high abundance of total rare earth elements ($\Sigma REE_{Exoskeleton}$ = 18.029 and ΣREE_{Matrix} = 31.780). In the exoskeletons, despite the homogeneous pattern observed in Figure 6, there is an enrichment of light rare earth elements (Nb_N/Yb_N = 2.053 and Pr_N/Yb_N = 2.211) and a depletion of medium rare earth elements (Nd_N/Dy_N = 1.314) with respect to heavy rare earth elements. Additionally, there are slightly positive anomalies of Europium (Eu/Eu* = 1.392 ± 0.101).

Table 3. Average Values of Rare Earth Elements and Analyzed Indices.

	^{57}La	^{58}Ce	^{59}Pr	^{60}Nd	^{62}Sm	^{63}Eu	^{64}Gd	^{65}Tb	^{66}Dy	^{39}Y	^{67}Ho	^{68}Er	^{69}Tm	^{70}Yb	^{71}Lu
Matrix	2.28	2.27	2.20	1.99	2.34	2.80	2.24	2.12	2.06	2.12	2.01	1.89	1.81	1.81	1.72
Exoskeleton	1.17	1.41	1.41	1.29	1.55	2.06	1.41	1.26	1.02	1.10	0.992	0.897	0.809	0.849	0.808

				INDICES								
					ΣREE		Eu/Eu*		REE_L/REE_P		REE_M	REE_P
	Rb/Sr	**Mn/Sr**	**Sr (ppm)**	$\bar{x}$	**max**	**min**	**value**	**error**	**Nb/Yb**	**Pr/Yb**	**Nd/Dy**	**Tb/Yb**
Matrix	0.40	1.36	2517.30	31.78	68.76	13.40	1.20	0.079	1.04	1.16	0.947	1.08
Exoskeleton	0.03	0.85	2220.62	18.03	25.39	9.69	1.39	0.101	2.05	2.21	1.31	1.85

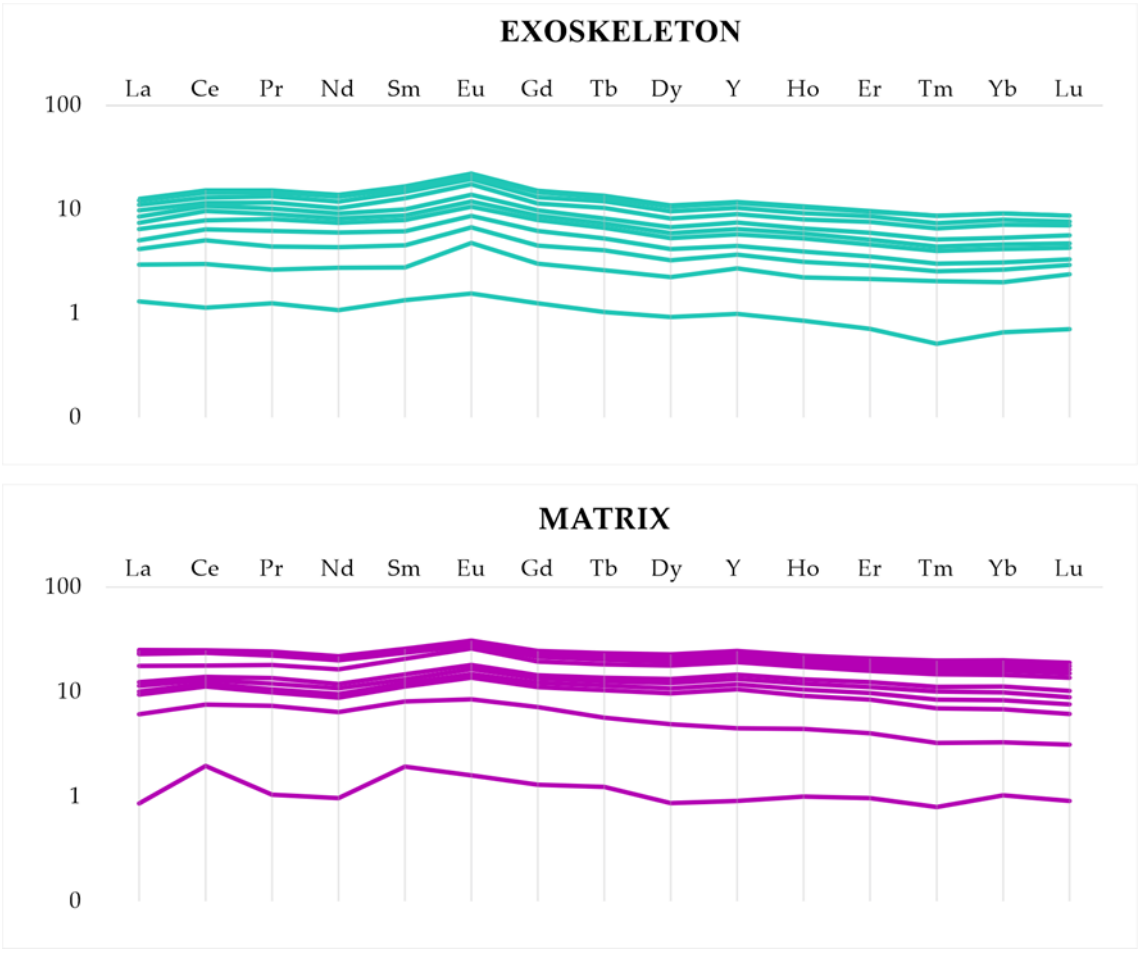


Figure 6. REE pattern of the studied sample, normalized to PAAS [50].

In the matrix, the observed pattern is like that of the exoskeletons, with enrichment of light rare earth elements (Nb_N/Yb_N = 1.035 and Pr_N/Yb_N = 1.159) and a slight depletion of medium rare earth elements (Nd_N/Dy_N = 0.947) with respect to heavy rare earth elements. Additionally, there are slightly positive anomalies of Europium (Eu/Eu* = 1.201 ± 0.079).

4.4. Sr, C, and O Stable Isotopes

The weighted average $^{87}Sr/^{86}Sr$ value obtained for the matrix was 0.70903 ± 0.00009 (2s, MSWD = 2), while it was 0.70885 ± 0.00002 (2s, MSWD = 1) for the exoskeletons of *Corumbella werneri*. The $^{87}Sr/^{86}Sr$ values of the matrix were more radiogenic than those of the exoskeletons.

The $\delta^{13}C$ results show a slight variation between the matrix and the exoskeletons, ranging between 3.98 and 4.26‰ in the former and 3.77 to 4.91‰ in the latter. As for the

$\delta^{18}O$ values, they range from −10.99 to −11.56‰ in the matrix and between −10.95 and −11.55‰ in the exoskeletons (VPDB).

The graphs in Figure 7 represent the dispersion of the analyzed data. It is noticeable that the matrix and the exoskeletons exhibit similar signals for $\delta^{13}C$ and $\delta^{18}O$, whereas the signals of $^{87}Sr/^{86}Sr$, although only slightly different, are statistically significant. The dispersion of the $^{87}Sr/^{86}Sr$ values in the exoskeleton is very small, showing a reproducibility like that of the reference material Walnut Canyon (WC) [51]. On the other hand, the matrix shows much more dispersed $^{87}Sr/^{86}Sr$ values.

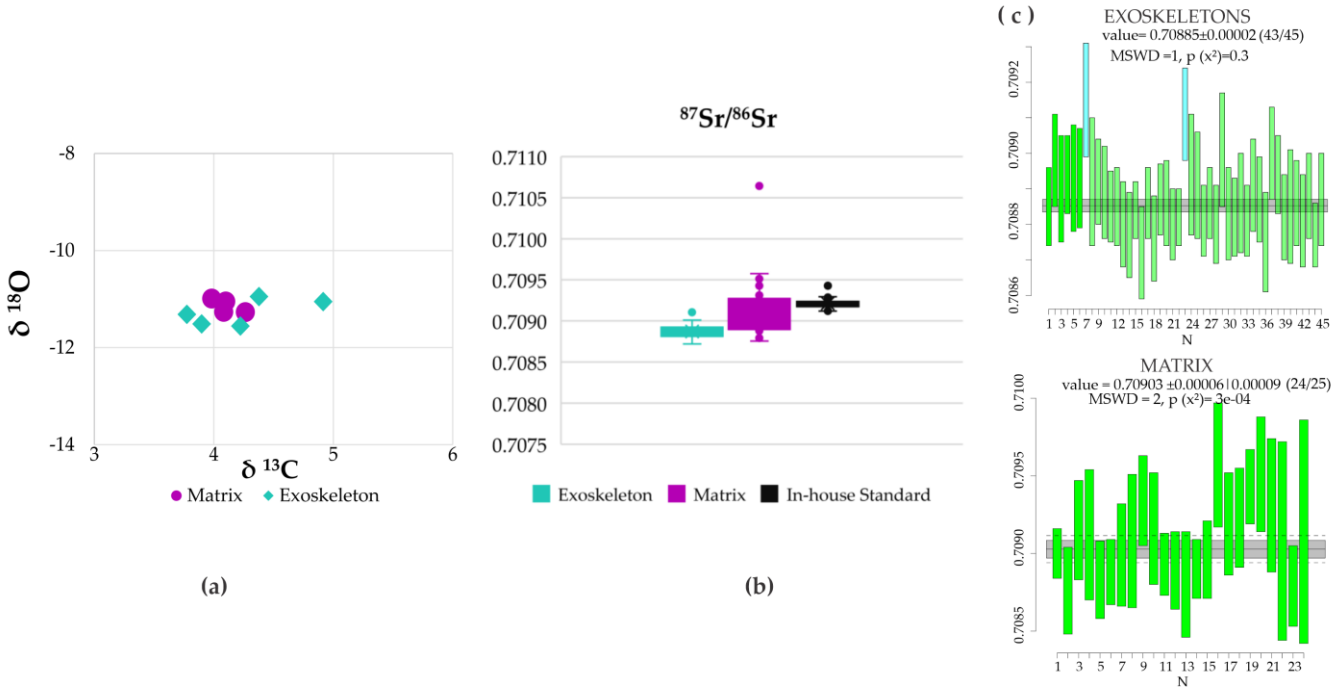


Figure 7. (**a**) Cross plot between carbon ($\delta^{13}C$) and oxygen ($\delta^{18}O$) isotope results from exoskeletons of *Corumbella werneri* (green diamonds) and the matrix (purple circles); (**b**) Boxplot of Strontium ($^{87}Sr/^{86}Sr$) isotope results from exoskeletons of *Corumbella werneri* and the matrix; (**c**) Weighted Media for Strontium ($^{87}Sr/^{86}Sr$) isotopes.

5. Discussion

Typically, Proterozoic rocks undergo isotopic alterations resulting from diagenetic and metamorphic processes. Considering this, several researchers such as [52–55] propose integrating lithochemical and isotopic data to determine the presence of potential modifying processes and the degree of alteration in the isotopic signal.

The isotopic composition of strontium (Figure 7b) exhibits a significant difference in the dispersion of the values between the matrix and the exoskeleton, as they are much more scattered in the former than in the latter. The slightly higher average and the larger dispersion of the values of the matrix may be attributed to the contribution of siliciclastic material, which is not present in the exoskeleton fragments. This indicates that the $^{87}Sr/^{86}Sr$ signal is mainly primary, as if there had been open system behavior, the detrital Sr would have contaminated the isotopic composition of the exoskeleton and increased the dispersion of the values.

The different composition of major and trace elements observed between the exoskeletons and the matrix, with a very low abundance of metals in the former, indicates that there was no significant exchange of elements between the two types of constituents during diagenesis. The abundance of clay minerals in the exoskeleton of *Corumbella werneri* is below the detection limit, so they could not be studied statistically. This, however, indicates that clay mineral contamination was neglectable. Additionally, the graphs shown in Figure 5 and Tables 1 and 2 show a clearly different chemical composition between the two types

of constituents, with the matrix more enriched in elements of siliciclastic origin due to its marly composition. This indicates that there has been no significant exchange of elements, so the effect of diagenesis has not been notably significant.

Additionally, the exoskeletons exhibit Mn/Sr averages of 0.85, Rb/Sr of 0.02, and a Sr concentration of 2220 ppm. The authors of [53] proposed that strontium isotope values in Neoproterozoic carbonates can be considered primary when Mn/Sr < 2, Rb/Sr < 0.005, and the Sr concentration is between 150 and 2500 ppm. Despite having a slightly higher Rb/Sr, the values of these parameters in the exoskeletons of this study align with the criteria of [53] for a primary signal. Furthermore, the $^{87}Sr/^{86}Sr$ values of the exoskeletons also agree with those proposed by [56] for the end of the Ediacaran period.

These observations suggest that the Sr isotopic composition of both the matrix and the exoskeletons is primary, as a diagenetic alteration would have homogenized the isotopic signal between the constituents and altered the lithogeochemical parameters. The $^{87}Sr/^{86}Sr$ values of the exoskeletons are also consistent with data from bulk rocks of the carbonate facies of the Tamengo Formation, ranging from 0.70848 to 0.70892 [57]; 0.7084 to 0.7085 [58]; 0.7084 to 0.7085 [23]; and 0.7085 to 0.7089 [59], as well as with the coeval Itapucumi Group in Paraguay, which presents 0.708604 [60].

In [55] the authors observed that diagenesis and metamorphism often increase Mn content and decrease Sr content in sedimentary rocks. The authors also suggest that Mn/Sr values < 1.5 and $\delta^{18}O > -10‰$ (VPDB) may indicate a primary origin of the carbon isotopic composition. As previously discussed, and considering the absence of primary Mn minerals, the studied sample exhibits average Mn/Sr values of 1.360 in the matrix and 0.849 in the exoskeletons, along with average $\delta^{18}O$ values of −11.15 and −11.28 (VPDB) in the matrix and in the exoskeletons, respectively. These values may indicate negligible chemical alteration during diagenesis, which is also testified by the absence of significant secondary features observed in the petrography. Therefore, the $\delta^{13}C$ values can reflect the composition of the inorganic carbon dissolved in the water of the sedimentary environment. These considerations about the signature of various geochemical parameters, alongside the texture observed in the microprobe images (Figure 3), also corroborate that *Corumbella werneri* had a carbonate exoskeleton, as proposed by [32] and differently from [61], which considered it organic.

The oxygen isotope exhibits extremely low values in both the matrix and the exoskeletons, consistent with most of those documented for the Neoproterozoic, e.g., [4,62–65]. Extremely low $\delta^{18}O$ values are commonly interpreted as the result of meteoric diagenesis; however, the reason why they are widespread in the Neoproterozoic is still unclear. Considering the absence of evidence of meteoric diagenesis in the studied sample, and the controversial origin of low $\delta^{18}O$ values in the Neoproterozoic, we do not have adequate information to make a conclusive interpretation of the $\delta^{18}O$ values in this case study.

On the other hand, the $\delta^{13}C$ data can contribute to the understanding of the living conditions of *Corumbella werneri.* As discussed above, the origin of the signal is mainly primary; therefore, the similarity of the carbon isotopic values between the micrite in the matrix and the exoskeletons suggests that these two constituents formed under the same environmental conditions. Iron speciation data in a recent study by [66] suggest that the depositional environment of the Tamengo Formation was mainly anoxic. However, the presence of fragments of *Cloudina lucianoi* and *Corumbella werneri,* which needed oxygen to survive, led to the interpretation that the water column was sufficiently oxygenated, but there was a sharp chemocline near the bottom where the conditions turned anoxic [66].

In Neoproterozoic carbonate platforms, micrite was produced by microbial mats and then swept and redeposited in deeper and calmer settings nearby, e.g., [67]. Additionally, the exoskeletons of *Corumbella werneri* are extremely thin and, therefore, fragile and easy to disintegrate by clastic transport. The exoskeletons in the studied sample occur in relatively large (mm size) fragments, and thus may not have been transported for a long distance after the death of the organism [28]. This suggests that *Corumbella werneri* lived in low energy conditions, near microbial carbonate mounds that produced micrite. Moreover, considering

that the average $\delta^{13}C$ values of bulk carbonate facies in the Tamengo Formation are between 5‰ and 6‰ [26], the slightly lower values recorded in the exoskeletons of *Corumbella werneri* and the micrite in-between indicate that they formed in conditions slightly deeper than the main carbonate factory, where the recycling of C was slightly slower (Figure 8A). This interpretation corroborates those of previous authors based on sedimentological and stratigraphic analyses, which proposed that the marly-to-shaly intervals with fossils of *Corumbella werneri* in the Tamengo Formation represent an environment just below the storm wave base, with some high-energy episodes that provided oxygen to the *Corumbella werneri*. This setting was deeper and calmer than that of most of the carbonate deposits of the Tamengo Formation, which display frequent hummocky cross-lamination and bioclasts of *Cloudina lucianoi* [27,28]. The dwelling environment of the *Corumbella werneri* was also situated above a sharp chemocline, which separated it from the anoxic bottom beneath [66]. After the death of the organisms, the exoskeletons got transported by gravity and deposited below the storm wave base, together with micrite and siliciclastic mud coming from the continent, which formed the marly matrix (Figure 8B).

The concentrations of REEs observed in the sample of this study exhibit a relatively homogeneous pattern between light and heavy REEs. However, there is evident enrichment in light elements both in the matrix and in the exoskeletons. Studies conducted on carbonate exoskeletons in paleoenvironments comparable to those of the present study show normalized values of 1 or lower [68–71]. The sample studied here, however, presents values in both the matrix and exoskeletons that are ten times higher. In addition, the analysis of REEs revealed the presence of Eu anomalies both in the matrix and the exoskeletons.

Europium is a unique element that remains stable under high temperatures, high pressures, and extremely reducing environments. In addition, it enters the carbonate minerals in equilibrium with the seawater, where it then becomes rather immobile [72]. To our knowledge, there are no environmental or diagenetic mechanisms that can explain such Eu anomalies in carbonate sediments. The authors of [73,74] suggest that positive Eu anomalies would be due to post-depositional alterations associated with hydrothermal processes. On the other hand, [75] explores the possibility that positive variations of this element are correlated with a mineralogical assemblage rich in feldspar. The sample analyzed in this study presents a subtle positive anomaly quantified for the matrix at $Eu/Eu^* = 1.201 \pm 0.079$ and for the exoskeletons at $Eu/Eu^* = 1.392 \pm 0.101$. Despite what was proposed by [75], the mineralogy shown in the QEMSCAN data, along with the analysis of major elements in the matrix and exoskeletons, allows us to exclude the presence of abundant feldspar and thus interpret the Eu signature as related to post-depositional hydrothermal influence.

The rare REEs' data of the studied sample do not represent primary values consistent with carbonates and fossils from similar environments, e.g., [68–71], and the Eu anomalies suggest post-depositional hydrothermal alteration. Data acquired from calorimetric analyses by [76], using the thermal alteration index (TAI) methodology, obtained temperatures between >150 °C and <200 °C [77] consistent with a hydrothermal context. On the other hand, no discernible hydrothermal features, such as recrystallization, mineral transformation, and new mineral growth, were observed in the petrography, nor were there hydrothermal signatures in the Sr and O stable isotopes.

Despite the evidence of hydrothermal influence being controversial, we could not identify other reasonable explanations for the REEs' values and the Eu anomalies both in the matrix and in the exoskeleton. Consequently, we hypothesize that a hydrothermal alteration happened during the late diagenesis by diffusion at the regional scale, and so did not affect the texture of the studied sample (Figure 8C). Apparently, both the $^{87}Sr/^{86}Sr$ and the $\delta^{18}O$ were not sensitive to this regional diffusion. Additionally, ref. [25] observed macroscopic fluorite crystal occurring punctually in the lower part of the Tamengo Formation in the Laginha Section, which may be related to hydrothermal and subvolcanic processes. Evidence of a hydrothermal event in the region was also found in the rocks of the Jacadigo Group and was dated at the earliest Cambrian [78]. The occurrence of

hydrothermal activity soon after the deposition of the Tamengo Formation, if confirmed, may reinforce the hypothesis of [26], placing the Tamengo Formation in a post-rift context, but still influenced by active tectonics. It may also explain the different thermal alterations in the clay minerals between the Tamengo and the overlying Guaicurus Formation observed by [79].

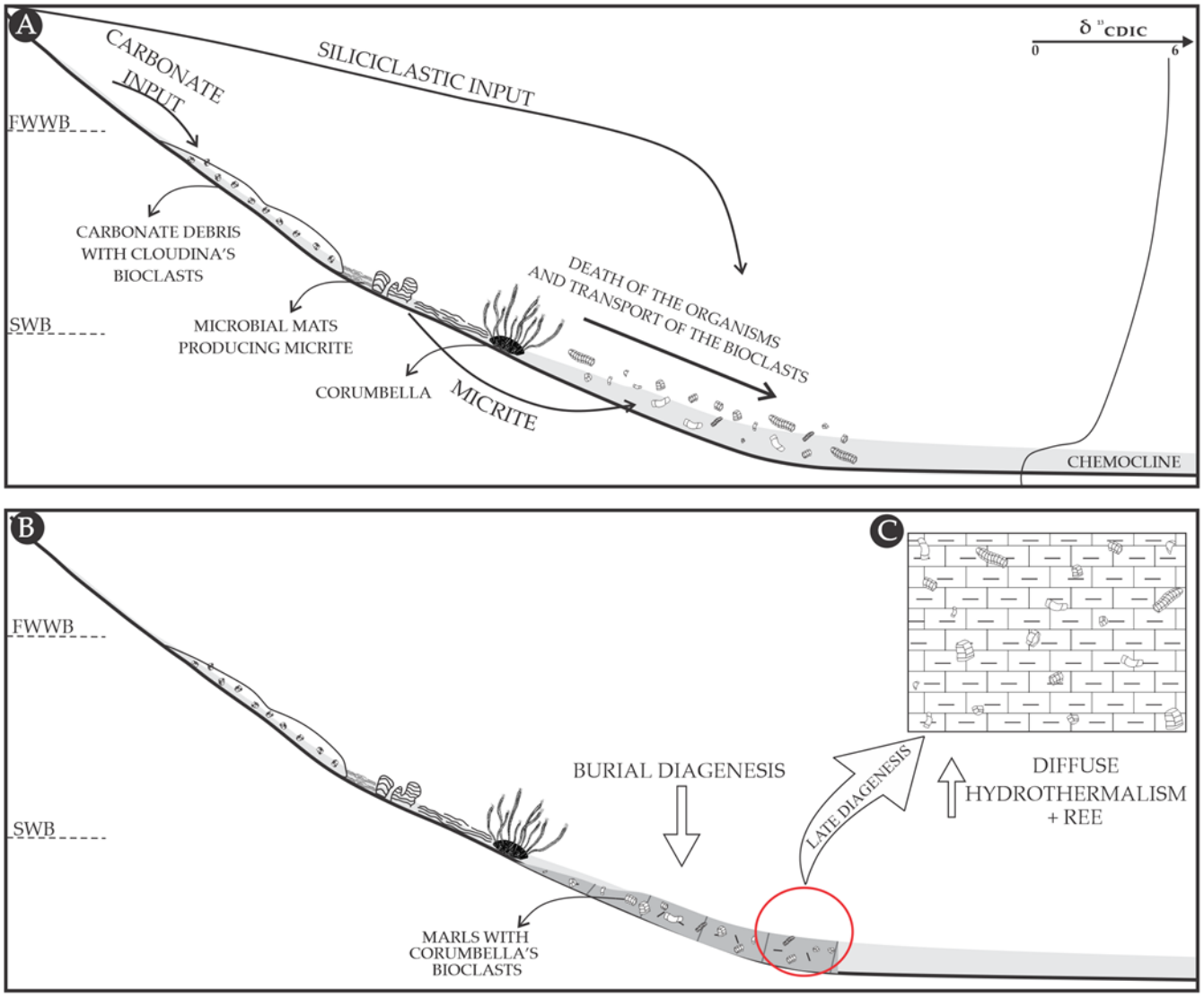


Figure 8. Schematic drawing of the evolutionary history of the rock. (**A**) Deposition environment, where micrite producers are observed, along with carbonate and silica inputs, which later transport and formed the studied rock; (**B**) Burial diagenetic process, characterized by the lithification of rock; (**C**) Late diagenesis, characterized by a diffuse hydrotermalism with REE enrichment. The reconstruction of *Corumbella werneri* depicted in the figures is sourced from [61], FWWB—Fair weather wave base level; SWB—Storm wave base level.

6. Conclusions

The petrographic, mineralogical, geochemical, and isotopic information obtained from a sample of marl with well-preserved fragments of *Corumbella werneri* allowed for the unraveling the syn- and post-depositional signals of the Tamengo Formation, formed at the end of the Neoproterozoic. The absence of typical diagenetic textural features, such as recrystallization, mineral alteration, or crystallization of new minerals, combined with chemical parameters obtained from the matrix and the fossil exoskeletons, separately, indicated that the strontium and carbon isotopic compositions are mainly primary. This

evidence allowed us to constrain the living conditions of *Corumbella werneri* to a quiet environment, proximal to the storm wave base and just above the chemocline.

Another important finding of this study revealed a pattern of enrichment in total rare earth elements (REEs) and the presence of europium anomalies, suggesting hydrothermal influence during the late diagenesis. Although it affected the elemental composition of the rocks, it did not alter the texture and the isotopic compositions of Sr and O in the carbonate. Probably, this process occurred by diffusion at the regional scale, resulting in remarkable REE enrichment in both the matrix and the exoskeletons.

The results and interpretations presented in this work, although based on a pilot study with only one sample, significantly contribute to the understanding of the geological processes that affected the Tamengo Formation and the exoskeletons of *Corumbella werneri*, providing new insights into the environmental and diagenetic conditions during the Neoproterozoic. Additionally, it highlights the importance of a multiproxy approach to unravel the complex mixture of signals recorded in a carbonate sedimentary rock.

Supplementary Materials: The following supporting information can be downloaded at: https://www.mdpi.com/article/10.3390/min14080784/s1, Figure S1: Strontium Spots of *Corumbella werneri*; Figure S2: Strontium Spots of matrix; Figure S3: Microprobe Imagens; Table S1: Elementary Geochemistry of Matrix; Table S2: Elementary Geochemistry of *Corumbella werneri*; Table S3: Carbon and Oxygen Isotopes values; Table S4: Strontium Isotopes values; Table S5: REE values; Table S6: REE normalized values; Table S7: Trace Values.

Author Contributions: A.V.A.C.A. methodology, investigation and writing—original draft preparation; M.G. supervision, project administration, review and editing; D.H.G.W. Field Supervision, Sample Collection and review; D.A.D.C. micropaleontology laboratory coordinator, funding acquisition and review; G.d.O.G. geochemical data curation and review. All authors have read and agreed to the published version of the manuscript.

Funding: This study was financed in part by the Coordenação de Aperfeiçoamento de Pessoal de Nível Superior–Brasil (CAPES)–Finance Code 001 and process n. 88887.635540/2021-00, by the Research Foundation of the Federal District (FAPDF)–process no. 0193.001609/2017, and by the project "Arcabouço cronobioestratigráfico do Ediacariano do Brasil através do desenvolvimento metodológico em paleontologia–EDIACARIANO", funded by ANP & PETROBRAS, N. PETROBRAS/FUB-IG-2012/5005. D. Do Carmo thanks CNPq for research his grant 309805/2021-0.

Data Availability Statement: The original contributions presented in the study are included in the article/Supplementary Materials, further inquiries can be directed to the corresponding authors.

Acknowledgments: The Micropaleontology Laboratory at the University of Brasília generously provided the sample for this study. We thank Matheus Denezine for the assistance with the selection of the sample. We are also thankful to André Alvim for the assistance with the C and O isotopes analyses, Paola Barbosa for the QemScan analysis, and Iris Dias Santos for the SEM and electron microprobe analyses.

Conflicts of Interest: The authors declare no conflict of interest.

References

1. Cohen, K.M.; Finney, S.C.; Gibbard, P.L.; Fan, J.X. The ICS International Chronostratigraphic Chart. *Episodes* **2013**, *36*, 199–204. [CrossRef] [PubMed]
2. Hayes, J.M.; Strauss, H.; Kaufman, A.J. The abundance of 13 C in marine organic matter and isotopic fractionation in the global biogeochemical cycle of carbon during the past 800 Ma. *Chem. Geol.* **1999**, *161*, 103–125. [CrossRef]
3. Hoffman, P.F.; Schrag, D.P. The snowball Earth hypothesis: Testing the limits of global change. *Terra Nova* **2002**, *14*, 129–155. [CrossRef]
4. Halverson, G.P.; Hoffman, P.F.; Schrag, D.P.; Maloof, A.C.; Rice, A.H.N. Toward a Neoproterozoic composite carbon-isotope record. *Bull. Geol. Soc. Am.* **2005**, *117*, 1181–1207. [CrossRef]
5. Halverson, G.P.; Shields-Zhou, G. Chapter 4: Chemostratigraphy and the Neoproterozoic glaciations. *Geol. Soc. Mem.* **2011**, *36*, 51–66. [CrossRef]
6. Lyons, T.W.; Reinhard, C.T.; Planavsky, N.J. The rise of oxygen in Earth's early ocean and atmosphere. *Nature* **2014**, *506*, 307–315. [CrossRef] [PubMed]

7. Grotzinger, J.P.; Fike, D.A.; Fischer, W.W. Enigmatic origin of the largest-known carbon isotope excursion in Earth's history. *Nat. Geosci.* **2011**, *4*, 285–292. [CrossRef]
8. Catuneanu, O.; Eriksson, P.G. Sequence stratigraphy of the Precambrian. *Gondwana Res.* **2007**, *12*, 560–565. [CrossRef]
9. Shieh, Y.N.; Taylor, H.P. Oxygen and Carbon Isotope Studies of Contact Metamorphism of Carbonate Rocks. *J. Petrol.* **1969**, *10*, 307–331. [CrossRef]
10. Kaufman, A.J.; Knoll, A.H. Neoproterozoic variations in the C-isotopic composition of seawater: Stratigraphic and biogeochemical implications. *Precambrian Res.* **1995**, *73*, 27–49. [CrossRef]
11. Almeida, F.F.M. Provincia Tocantins, Setor Sudoeste. In *O Pré-Cambriano do Brasil*; Hasui, Y., Ed.; Edgard Blucher: São Paulo, Brazil, 1984; pp. 265–281.
12. Boggiani, P.C.; Fairchild, T.R.; Coimbra, A.M. O Grupo Corumbá (Neoproterozóico- Cambriano) na Região Central da Serra da Bodoquena (Faixa Paraguai), Mato Grosso do Sul. *Rev. Bras. Geociências* **1993**, *23*, 301–305. [CrossRef]
13. Boggiani, P.C. Análise Estratigráfica da Bacia Corumbá (Neoproterozóico)–Mato Grosso do Sul. Ph.D. Thesis, Universidade de São Paulo, São Paulo, Brazil, 1998.
14. Hahn, G.; Hahn, R.; Leonardos, O.H.; Pflug, H.D.; Walde, D.H.G. Körperlich erhaltene Scyphozoen-Reste aus dem Jungpräkambrium Brasiliens. *Geol. Palaeontol.* **1982**, *16*, 1–18.
15. Beurlen, K.; Sommer, F.W. Observações estratigráficas e paleontológicas sobre o Calcário Corumbá. *Serv. Graf. Inst. Bras. Geogr. Estat. Rio Jan.* **1957**, *168*, 18.
16. Adôrno, R.R.; Walde, D.H.G.; Erdtmann, B.D.; Denezine, M.; Cortijo, I.; Do Carmo, D.A.; Giorgioni, M.; Ramos, M.E.A.F.; Fazio, G. First occurrence of Cloudina carinata Cortijo et al., 2010 in South America, Tamengo Formation, Corumbá Group, upper Ediacaran of Midwestern. *Estud. Geológicos* **2019**, *75*, 95. [CrossRef]
17. Adorno, R.R.; do Carmo, D.A.; Germs, G.; Walde, D.H.G.; Denezine, M.; Boggiani, P.C.; e Silva, S.C.S.; Vasconcelos, J.R.; Tobias, T.C.; Guimarães, E.M.; et al. Cloudina lucianoi (Beurlen & Sommer, 1957), Tamengo Formation, Ediacaran, Brazil: Taxonomy, analysis of stratigraphic distribution and biostratigraphy. *Precambrian Res.* **2017**, *301*, 19–35.
18. Almeida, F.F.M. Geologia da Serra da Bodoquena (Mato Grosso), Brasil. Boletim da Divisão de Geologia e Mineralogia. *DNPM* **1965**, *117*, 1–96.
19. Boggiani, P.C.; Alvarenga, C.J.S. Faixa Paraguai. In *Geologia do Continente Sul-Americano: Evolução da obra de Fernando Flávio Marques de Almeida Becca*; Mantesso-Neto, V., Bartorelli, A., Carneiro, C.D.R., Brito-Neves, B.B., Eds.; DNPM: Port Moresby, Papua New Guinea, 2004; pp. 113–121.
20. Babinski, M.; Boggiani, P.C.; Trindade, R.I.F.; Fanning, C.M. Detrital zircon ages and geochronological constraints on the Neoproterozoic Puga diamictites and associated BIFs in the southern Paraguay Belt, Brazil. *Gondwana Res.* **2013**, *23*, 988–997. [CrossRef]
21. Boggiani, P.C. *Sedimentação Autigênica Neoproterozóica e Mineralizações Associadas–Um Registro não Uniformitarista*; Tese de Livre Dociência, Universidade de São Paulo: São Paulo, Brazil, 2010.
22. Boggiani, P.C.; Gaucher, C.; Sial, A.N.; Babinski, M.; Simon, C.M.; Riccomini, C.; Ferreira, V.P.; Fairchild, T.R. Chemostratigraphy of the Tamengo Formation (Corumbá Group, Brazil): A contribution to the calibration of the Ediacaran carbon-isotope curve. *Precambrian Res.* **2010**, *182*, 382–401. [CrossRef]
23. Babinski, M.; Boggiani, P.C.; Fanning, C.M.; Fairchild, T.R.; Simon, C.M.; Sial, A.N. U-Pb Shrimp Geochronology and Isotope Chemostratigraphy (C, O, Sr) of the Tamengo Formation, Southern Paraguay Belt, Brazil. In *VI South American Symposium on Isotope Geology*; Sociedade Brasileira de Geologia: San Carlos de Bariloche, Argentina, 2008; p. 160.
24. Parry, L.A.; Boggiani, P.C.; Condon, D.J.; Garwood, R.J.; Leme, J.D.M.; McIlroy, D.; Brasier, M.D.; Trindade, R.; Campanha, G.A.; Pacheco, M.L.; et al. Ichnological evidence for meiofaunal bilaterians from the terminal Ediacaran and earliest Cambrian of Brazil. *Nat. Ecol. Evol.* **2017**, *1*, 1455–1464. [CrossRef]
25. Ramos, M.E.A.F. Sedimentological, Petrographic and geochemical characterization of Ediacaran platform carbonates (Tamengo Formation, Corumbá Group). Master's Thesis, Universidade de Brasília, Brasília, Brazil, 2019.
26. Ramos, M.E.A.F.; Giorgioni, M.; Walde, D.H.G.; do Carmo, D.A.; Fazio, G.; Vieira, L.C.; Denezine, M.; VSantos, R.; RAdôrno, R.; Lage Guida, L. New Facies Model and Carbon Isotope Stratigraphy for an Ediacaran Carbonate Platform From South America (Tamengo Formation—Corumbá Group, SW Brazil). *Front. Earth Sci.* **2022**, *10*, 749066. [CrossRef]
27. de Oliveira, R.S.; Nogueira, A.C.R.; Romero, G.R.; Truckenbrodt, W.; da Silva Bandeira, J.C. Ediacaran ramp depositional model of the Tamengo Formation, Brazil. *J. S. Am. Earth Sci.* **2019**, *96*, 102348. [CrossRef]
28. Amorim, K.B.; Afonso, J.W.L.; Leme, J.M.; Diniz, C.Q.C.; Rivera, L.C.M.; Gómez-Gutiérrez, J.C.; Boggiani, P.C.; Trindade, R.I.F. Sedimentary facies, fossil distribution and depositional settingof the late Ediacaran Tamengo Formation (Brazil). *Sedimentology* **2020**, *67*, 3422–3450. [CrossRef]
29. Pacheco, M.L.A.F.; Sanchez, E.A.M.; Soares, L.P.C.M.; Leme, J.M.; Fairchild, T.R. Interferências sobre Paleoambiente e associações paleoecológicas de Corumbella werneri. In *Anais do Congresso Brasileiro de Geologia*; Sociedade Brasileira de Geologia: Santos, Brazil, 2012.
30. Pacheco, M.L.F.; Galante, D.; Rodrigues, F.; de MLeme, J.; Bidola, P.; Hagadorn, W.; Stockmar, M.; Herzen, J.; Rudnitzki, I.D.; Pfeiffer, F.; et al. Insights into the Skeletonization, Lifestyle, and Affinity of the Unusual Ediacaran Fossil Corumbella. *PLoS ONE* **2015**, *10*, e0114219. [CrossRef] [PubMed]

31. Van Iten, H.; Marques, A.C.; de Leme, J.M.; Pacheco, M.L.A.F.; Simões, M.G. Origin and early diversification of the phylum Cnidaria Verrill: Major developments in the analysis of the taxon's Proterozoic-Cambrian history. *Palaeontology* **2014**, *57*, 677–690. [CrossRef]
32. Walde, D.H.G.; Weber, B.; Erdtmann, B.D.; Steiner, M. Taphonomy of Corumbella werneri from the Ediacaran of Brazil: Sinotubulitid tube or conulariid test? Alcheringa: An Australasian. *J. Palaeontol.* **2019**, *43*, 335–350.
33. Walde, D.H.G.; Do Carmo, D.A.; Guimarães, E.M.; Vieira, L.C.; Erdtmann, B.D.; Sanchez, E.A.M.; Adorno, R.R.; Tobias, T.C. New aspects of Neoproterozoic-Cambrian transition in the Corumbá region (state of Mato Grosso do Sul, Brazil). *Ann. Paleontol.* **2015**, *101*, 213–224. [CrossRef]
34. Delgado, F. Primary Textures in Dolostones and Recrystallized Limestones: A Technique for their Microscopic Study. *J. Sediment. Res.* **1977**, *47*, 1339–1341. [CrossRef]
35. Chapman, S.K. *Working with a Scanning Electron Microscope*; Lodgemark Press: Orpington, UK, 1986.
36. Jochum, K.P.; Weis, U.; Schwager, B.; Stoll, B.; Wilson, S.A.; Haug, G.H.; Andreae, M.O.; Enzweiler, J. Reference Values Following ISO Guidelines for Frequently Requested Rock Reference Materials. *Geostand. Geoanal. Res.* **2016**, *40*, 333–350. [CrossRef]
37. Gonçalves, G.O.; Lana, C.; Scholz, R.; Buick, I.S.; Gerdes, A.; Kamo, S.L.; Corfu, F.; Rubatto, D.; Wiedenbeck, M.; Nalini, H.A., Jr.; et al. The Diamantina Monazite: A New Low-Th Reference Material for Microanalysis. *Geostand. Geoanal. Res.* **2018**, *42*, 25–47. [CrossRef]
38. Chew, D.M.; Babechuk, M.G.; Cogné, N.; Mark, C.; O'Sullivan, G.J.; Henrichs, I.A.; Doepke, D.; McKenna, C.A. (LA,Q)-ICPMS trace-element analyses of Durango and McClure Mountain apatite and implications for making natural LA-ICPMS mineral standards. *Chem. Geol.* **2016**, *435*, 35–48. [CrossRef]
39. Paton, C.; Hellstrom, J.; Paul, B.; Woodhead, J.; Hergt, J. Iolite: Freeware for the visualisation and processing of mass spectrometric data. *J. Anal. At. Spectrom.* **2011**, *26*, 2508. [CrossRef]
40. Craig, H. Isotopic standards for carbon and oxygen and correction factors for mass-spectrometric analysis of carbon dioxide. *Geochim. Cosmochim. Acta* **1957**, *12*, 133–149. [CrossRef]
41. Yang, Y.H.; Wu, F.Y.; Wilde, S.A.; Liu, X.M.; Zhang, Y.B.; Xie, L.W.; Yang, J.H. In situ perovskite Sr–Nd isotopic constraints on the petrogenesis of the Ordovician Mengyin kimberlites in the North China Craton. *Chem. Geol.* **2009**, *264*, 24–42. [CrossRef]
42. Yang, Y.H.; Wu, F.Y.; Li, Y.; Yang, J.H.; Xie, L.W.; Liu, Y.; Zhang, Y.B.; Huang, C. In situ U–Pb dating of bastnaesite by, L.A.-I.C.P.-M.S. *J. Anal. At. Spectrom.* **2014**, *29*, 1017–1023. [CrossRef]
43. DePaolo, D.J.; Ingram, B.L. High-Resolution Stratigraphy with Strontium Isotopes. *Science* **1985**, *227*, 938–941. [CrossRef] [PubMed]
44. El Meknassi, S.; Dera, G.; Cardone, T.; De Rafélis, M.; Brahmi, C.; Chavagnac, V. Sr isotope ratios of modern carbonate shells: Good and bad news for chemostratigraphy. *Geology* **2018**, *46*, 1003–1006. [CrossRef]
45. Roberts, N.M.W.; Rasbury, E.T.; Parrish, R.R.; Smith, C.J.; Horstwood, M.S.A.; Condon, D.J. A calcite reference material for LA-ICP-MS U-Pb geochronology. *Geochem. Geophys. Geosystems* **2017**, *18*, 2807–2814. [CrossRef]
46. Mulder, J.; Hagen-Peter, G.; Ubide, T.; Andreasen, R.; Kooijman, E.; Kielman-Schmitt, M.; Feng, Y.X.; Paul, B.; Karlsson, A.; Tegner, C.; et al. New Reference Materials, Analytical Procedures and Data Reduction Strategies for Sr Isotope Measurements in Geological Materials by LA-MC-ICP-MS. *Geostand. Geoanal. Res.* **2023**, *47*, 311–336. [CrossRef]
47. Dunham, R.J. Classification of Carbonate Rocks According to Depositional Textures. In *Classification of Carbonate Rocks*; Ham, W.E., Ed.; AAPG: Tulsa, OK, USA, 1962; pp. 108–121.
48. Flügel, E. *Microfacies of Carbonate Rocks*, 2nd ed.; Munnecke, A., Ed.; Springer: Berlin/Heidelberg, Germany, 2010; Volume 1, pp. 1–984.
49. Tostevin, R.; Wood, R.A.; Shields, G.A.; Poulton, S.W.; Guilbaud, R.; Bowyer, F.; Penny, A.M.; He, T.; Curtis, A.; Hoffmann, K.H.; et al. Low-oxygen waters limited habitable space for early animals. *Nat. Commun.* **2016**, *7*, 12818. [CrossRef] [PubMed]
50. Pourmand, A.; Dauphas, N.; Ireland, T.J. A novel extraction chromatography and MC-ICP-MS technique for rapid analysis of REE, Sc and Y: Revising CI-chondrite and Post-Archean Australian Shale (PAAS) abundances. *Chem. Geol.* **2012**, *291*, 38–54. [CrossRef]
51. Rasbury, E.T.; Present, T.M.; Northrup, P.; Tappero, R.V.; Lanzirotti, A.; Cole, J.M.; Wooton, K.M.; Hatton, K. Tools for uranium characterization in carbonate samples: Case studies of natural U–Pb geochronology reference materials. *Geochronology* **2021**, *3*, 103–122. [CrossRef]
52. Brand, U.; Veizer, J. Chemical Diagenesis of a Multicomponent Carbonate System -2: Stable Isotopes. *SEPM J. Sediment. Res.* **1981**, *51*, 987–997.
53. Jacobsen, S.B.; Kaufman, A.J. The Sr, C and O isotopic evolution of Neoproterozoic seawater. *Chem. Geol.* **1999**, *161*, 37–57. [CrossRef]
54. Kaufman, A.J.; Jacobsen, S.B.; Knoll, A.H. The Vendian record of Sr and C isotopic variations in seawater: Implications for tectonics and paleoclimate. *Earth Planet Sci. Lett.* **1993**, *120*, 409–430. [CrossRef]
55. Frimmel, H.E.; Fölling, P.G. Late Vendian Closure of the Adamastor Ocean: Timing of Tectonic Inversion and Syn-orogenic Sedimentation in the Gariep Basin. *Gondwana Res.* **2004**, *7*, 685–699. [CrossRef]
56. Halverson, G.P.; Dudás, F.Ö.; Maloof, A.C.; Bowring, S.A. Evolution of the 87Sr/86Sr composition of Neoproterozoic seawater. *Palaeogeogr. Palaeoclim. Palaeoecol.* **2007**, *256*, 103–129. [CrossRef]

57. Chang, H.K.; Kawashita, K.; Zaine, M.F. Isotopic Composition of carbonates from late proterozoic sucessions in Brazil and their stratigraphic variation. In Proceedings of the 14th International Sedimentological Congress, Recife, Brazil, 24–25 August 1994.
58. Sial, A.N.; Boggiani, P.C.; Babinski, M.; Ferreira, M.; Fairchild, T. *Negative C-Isotope Anomaly in the Ediacaran Tamengo Formation (Corumbá Group, Southern Paraguay Belt) (Abstract)*; International Geological Congress: Washington, DC, USA, 2008.
59. Gomez, G.J.C.; Paula-Santos, G.M.; Borges, A.K.; Guacaneme, C.; Caetano-Filho, S.; Babinski, M.; Trindade, R.I.F.D. C-O-Sr Isotopes in Tamengo Formation (Corumbá Group) at Laginha Mine section, southern Paraguay Belt, Brazil. In *49º Congresso Brasileiro de Geologia*; Sociedade Brasileira de Geologia: Rio de Janeiro, Brazil, 2018.
60. Warren, L.V.; Freitas, B.T.; Riccomini, C.; Boggiani, P.C.; Quaglio, F.; Simões, M.G.; Fairchild, T.R.; Giorgioni, M.; Gaucher, C.; Poire, D.G.; et al. Sedimentary evolution and tectonic setting of the Itapucumi Group, Ediacaran, northern Paraguay: From Rodinia break-up to West Gondwana amalgamation. *Precambrian Res.* **2019**, *322*, 99–121. [CrossRef]
61. Babcock, L.E.; Grunow, A.M.; Sadowski, G.R.; Leslie, S.A. Corumbella, an Ediacaran-grade organism from the Late Neoproterozoic of Brazil. *Palaeogeogr. Palaeoclim. Palaeoecol.* **2005**, *220*, 7–18. [CrossRef]
62. Jiang, G.; Kaufman, A.J.; Christie-Blick, N.; Zhang, S.; Wu, H. Carbon isotope variability across the Ediacaran Yangtze platform in South China: Implications for a large surface-to-deep ocean δ13C gradient. *Earth Planet Sci. Lett.* **2007**, *261*, 303–320. [CrossRef]
63. Knauth, L.P.; Kennedy, M.J. The late Precambrian greening of the Earth. *Nature* **2009**, *460*, 728–732. [CrossRef]
64. Macdonald, F.A.; Strauss, J.V.; Sperling, E.A.; Halverson, G.P.; Narbonne, G.M.; Johnston, D.T.; Kunzmann, M.; Schrag, D.P.; Higgins, J.A. The stratigraphic relationship between the Shuram carbon isotope excursion, the oxygenation of Neoproterozoic oceans, and the first appearance of the Ediacara biota and bilaterian trace fossils in northwestern Canada. *Chem. Geol.* **2013**, *362*, 250–272. [CrossRef]
65. Husson, J.M.; Higgins, J.A.; Maloof, A.C.; Schoene, B. Ca and Mg isotope constraints on the origin of Earth's deepest δ13C excursion. *Geochim. Cosmochim. Acta* **2015**, *160*, 243–266. [CrossRef]
66. Caxito, F.A.; Sperling, E.; Fazio, G.; Adorno, R.R.; Denezine, M.; Do Carmo, D.A.; Giorgioni, M.; Uhlein, G.J.; Sial, A.N. A shift in redox conditions near the Ediacaran/Cambrian transition and its possible influence on early animal evolution, Corumbá Group, Brazil. *Geosci. Front.* **2024**, *15*, 101810. [CrossRef]
67. Grotzinger, J.P.; James, N.P. Carbonate Sedimentation and Diagenesis in the Evolving Precambrian World. In *SEPM Society for Sedimentary Geology*; SEPM: Claremore, OK, USA, 2000; Volume 67.
68. Sholkovitz, E.; Shen, G.T. The incorporation of rare earth elements in modern coral. *Geochim. Cosmochim. Acta* **1995**, *59*, 2749–2756. [CrossRef]
69. Bellanca, A.; Masetti, D.; Neri, R. Rare earth elements in limestone/marlstone couplets from the Albian-Ccnomanian Cismon section (Venetian region, northern Italy)" assessing REE sensitivity to environmental changes. *Chem. Geol.* **1997**, *141*, 141–152. [CrossRef]
70. Zaky, A.H.; Brand, U.; Azmy, K.; Logan, A.; Hooper, R.G.; Svavarsson, J. Rare earth elements of shallow-water articulated brachiopods: A bathymetric sensor. *Palaeogeogr. Palaeoclim. Palaeoecol.* **2016**, *461*, 178–194. [CrossRef]
71. Valdés-Vilchis, S.; Sánchez-Beristain, F.; Bernal, J.P.; Juárez-Aguilar, E.A. Rare Earth Elements and Yttrium (REE+Y) patterns in recent Anadara brasiliana shells from Playa Norte, Barra de Cazones (Veracruz, Mexico): Evidence of anthropogenic contamination linked to river output? *J. S. Am. Earth Sci.* **2021**, *110*, 103368. [CrossRef]
72. Bau, M.; Dulski, P. Anthropogenic origin of positive gadolinium anomalies in river waters. *Earth Planet Sci. Lett.* **1996**, *143*, 245–255. [CrossRef]
73. Bau, M. Rare-earth element mobility during hydrothermal and metamorphic fluid-rock interaction and the significance of the oxidation state of europium. *Chem. Geol.* **1991**, *93*, 219–230. [CrossRef]
74. Frimmel, H.E. On the reliability of stable carbon isotopes for Neoproterozoic chemostratigraphic correlation. *Precambrian Res.* **2010**, *182*, 239–253. [CrossRef]
75. Madhavaraju, J.; González-León, C.M.; Lee, Y.I.; Armstrong-Altrin, J.S.; Reyes-Campero, L.M. Geochemistry of the Mural Formation (Aptian-Albian) of the Bisbee Group, Northern Sonora, Mexico. *Cretac Res.* **2010**, *31*, 400–414. [CrossRef]
76. Tobias, T.C. Micropaleontologia da Formação Tamengo, Eco Parque Cacimba da Saúde, Ediacarano, Grupo Corumbá, Estado do Mato Grosso do Sul, Brasil. Master's Thesis, Universidade de Brasília, Brasília, Brazil, 2014.
77. Staplin, F.L. *Determination of Thermal Alteration Index from Color of Exinite (Pollen, Spores)*; AAPG: Tulsa, OK, USA, 1982.
78. Piacentini, T.; Vasconcelos, P.M.; Farley, K.A. 40Ar/39Ar constraints on the age and thermal history of the Urucum Neoproterozoic banded iron-formation, Brazil. *Precambrian Res.* **2013**, *228*, 48–62. [CrossRef]
79. Fazio, G.; Guimarães, E.M.; Walde, D.W.G.; do Carmo, D.A.; Adorno, R.R.; Vieira, L.C.; Denezine, M.; da Silva, C.B.; de Godoy, H.V.; Borges, P.C.; et al. Mineralogical and chemical composition of Ediacaran-Cambrian pelitic rocks of The Tamengo and Guaicurus formations, (Corumbá Group–MS, Brazil): Stratigraphic positioning and paleoenvironmental interpretations. *J. S. Am. Earth Sci.* **2019**, *90*, 487–503. [CrossRef]

Disclaimer/Publisher's Note: The statements, opinions and data contained in all publications are solely those of the individual author(s) and contributor(s) and not of MDPI and/or the editor(s). MDPI and/or the editor(s) disclaim responsibility for any injury to people or property resulting from any ideas, methods, instructions or products referred to in the content.